Photosynthesis Research **66:** 45–56, 2000.

Emerging techniques

Airborne test of laser pump-and-probe technique for assessment of phytoplankton photochemical characteristics

Alexander M. Chekalyuk[1,*], Frank E. Hoge[2], Charles W. Wright[2], Robert N. Swift[3] & James K. Yungel[3]

[1]*National Research Council;* [2]*Goddard Space Flight Center;* [3]*EG & G, Inc., NASA Goddard Space Flight Center, Wallops Flight Facility, Wallops Island, VA 23337, USA;* [*]*Author for correspondence (e-mail: chekaluk@osb.wff.nasa.gov; fax: +1-757-824-1036)*

Received 16 December 1999; accepted in revised form 31 August 2000

Key words: chlorophyll, energy quenching, fluorescence, LIDAR, photochemistry, photosynthesis, Photosystem II, phytoplankton, pump and probe, remote sensing

Abstract

Initial results of the airborne LIDAR measurement of photochemical quantum yield, Φ_{Po}, and functional absorption cross-section, σ_{PSII}, of Photosystem II (PS II) are reported. NASA's AOL3 LIDAR was modified to implement short-pulse pump-and-probe (SP-P&P) LIDAR measurement protocol. The prototype system is capable of measuring a pump-induced increase in probe-stimulated chlorophyll fluorescence, $\Delta F/F_{sat}$, along with the acquisition of 'conventional' LIDAR-fluorosensor products from an operational altitude of 150 m. The use of a PS II sub-saturating probe pulse increases the response signal but also results in excessive energy quenching (EEQ) affecting the $\Delta F/F_{sat}$ magnitude. The airborne data indicated up to a 3-fold EEQ-caused decline in $\Delta F/F_{sat}$, and 2-fold variability in the EEQ rate constant over a spatial scale a few hundred kilometers. Therefore, continuous monitoring of EEQ parameters must be incorporated in the operational SP-P&P protocol to provide data correction for the EEQ effect. Simultaneous airborne LIDAR measurements of Φ_{Po} and σ_{PSII} with EEQ correction were shown to be feasible and optimal laser excitation parameters were determined. Strong daytime $\Delta F/F_{sat}$ decline under ambient light was found in the near-surface water layer over large aquatic areas. An example of SP-P&P LIDAR measurement of phytoplankton photochemical and fluorescent characteristics in the Chesapeake Bay mouth is presented. Prospects for future SP-P&P development and related problems are discussed.

Abbreviations: Chl – chlorophyll; E and E_{pm} – probe and pump pulse fluences (μmol quanta m^{-2}), respectively; EEQ – excessive energy quenching; EST – eastern standard time in the USA; F – intensity of Chl fluorescence stimulated by single probe laser pulse; F_{sat} – intensity of Chl fluorescence stimulated by probe pulse following PS II sub-saturating pump pulse with a 30 μs delay; $\Delta F/F_{sat} = (F_{sat} - F)/F_{sat}$ – relative pump-induced change in probe-stimulated Chl fluorescence yield; Φ_{Po} – maximal potential quantum yield of PS II photochemistry in the dark-adapted state; LIDAR – 'LIght Detection And Ranging', an abbreviation conventionally used for laser remote sensing technique; P&P – pump and probe (technique); PS II – Photosystem II; R_Q – relative EEQ rate parameter; R^2 – correlation coefficient; SP – short pulse ($\sim$ 10 ns); SD – standard deviation of errors; SE – standard error of estimate; σ_{PSII} – functional absorption cross-section per PS II reaction center

Introduction

An advantage of active fluorescence techniques, such as 'pump-and-probe' (P&P) (Mauzerall 1972; Falkowski et al. 1986; Kramer et al. 1990), 'fast repetition rate' (Falkowski and Kolber 1995; Kolber et al. 1998), 'pump during probe' (Olson et al. 1996) and 'pulse amplitude modulation' (Schreiber et al.

1975; Schreiber et al. 1993) is that they can provide information about important photochemical and photosynthetic characteristics. In particular, the rates of gross photosynthetic oxygen evolution and carbon fixation (i.e. primary productivity) can be estimated by using the magnitudes of the functional absorption cross-section and the PS II photochemical quantum yield measured by using the P&P technique (Kolber and Falkowski 1993; Falkowski and Kolber 1995). Airborne implementation of P&P technology would allow the fluorescence measurement of molecular photochemical processes for assessment of biological productivity and carbon fixation over large oceanic areas. The use of biophysical approaches may provide improved estimates of the biological 'carbon pump' in the Ocean, an essential component of the global carbon cycle (Field et al. 1998).

Shipboard submersible 'P&P' and 'fast-repetition-rate' fluorometers have significantly increased the capacity for studying phytoplankton photosynthesis in natural conditions (Kolber et al. 1990, 1994; Falkowski et al. 1991; Geider et al. 1993; Falkowski and Kolber 1995). A shipboard P&P LIDAR system demonstrated the potential of LIDAR sensors for monitoring of phytoplankton photochemical activity over a range of spatial and temporal scales (Chekalyuk and Gorbunov 1994a, b). A 'pump-during-probe' microscope and a flow cytometer provided new information about single-cell and group-specific phytoplankton photosynthetic characteristics in the sea (Chekalyuk et al. 1996; Olson et al. 1999). An attempt at airborne P&P LIDAR measurements (Johnson et al. 1995) confirmed its feasibility, but also emphasized sensitivity as a major limitation for its operational application.

A long-term 'strategic' goal of our research is to develop an airborne laser technology for monitoring phytoplankton photochemical characteristics, which can be operationally used as a part of an active-passive suite of instrumentation for fast and cost-efficient biomonitoring over large aquatic areas. Results from theoretical analyses and laboratory experiments have indicated that a short-pulse (SP) P&P protocol can be effectively utilized to eliminate the weak-probe limitation of the conventional P&P approach while significantly improving measurement sensitivity (Chekalyuk et al. 2000). The main objective of the research reported in this manuscript was to conduct an airborne test and optimization of the SP-P&P LIDAR measurement protocol. Initial information on spatial and temporal variability of phytoplankton photochemical and fluorescence characteristics within the Middle Atlantic Bight is presented along with the specific analytical results of the airborne SP-P&P LIDAR field tests. We consider this implementation of the SP-P&P LIDAR measurement protocol in the NASA AOL3 sensor as essentially a proof-of-concept experiment. Future research efforts with the SP-P&P LIDAR measurement protocol will be aimed at producing a practical airborne implementation that can be used to provide routine surveys of phytoplankton photochemical activity over wide areas.

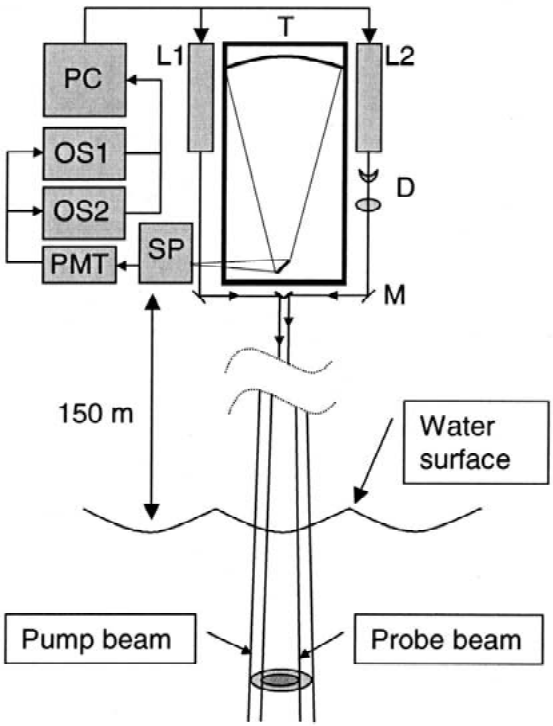

Figure 1. Block diagram of the prototype airborne SP-P&P LIDAR system. L1 and L2 – lasers, D – beam expander, M – adjustable folding mirror, T – telescope, SP – spectrograph, PMT – block of photomultipliers, OS1 and OS2 – digital oscilloscopes, PC – computer.

SP-P&P LIDAR prototype

The existing AOL3 system built at NASA Wallops Flight Facility was modified to permit the acquisition of airborne SP-P&P measurements from an operational altitude of 150 m. A block diagram of the instrument configuration is presented in Figure 1. The major modifications to the AOL3 sensor consisted of the addition of a second (pump) laser and corresponding changes in the hardware and software to accommo-

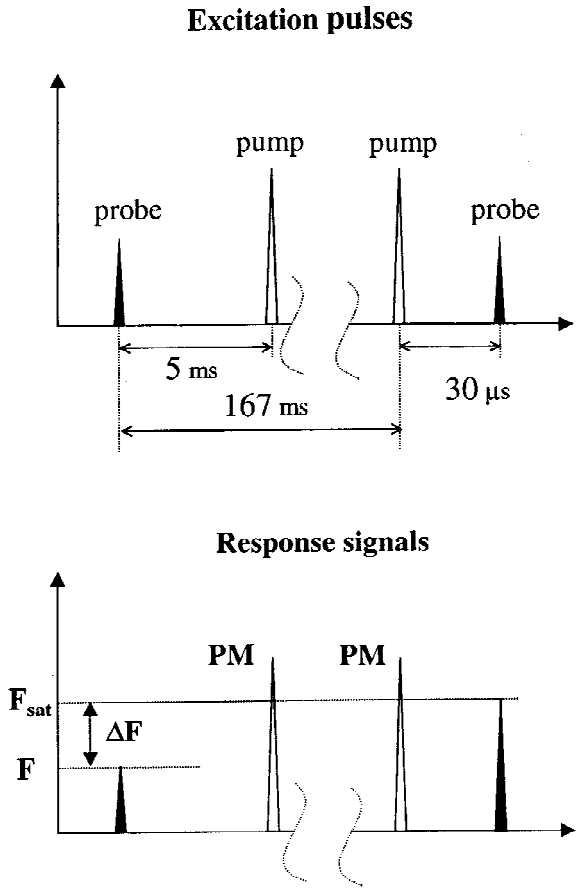

Figure 2. Timing diagram of the airborne SP-P&P measurements. Probe-pump and pump-probe laser pulse pairs (upper panel) alternately excite the water column. Black triangles in the lower panel are probe-stimulated Chl fluorescence from the probe-pump, F, and pump-probe, F_{sat}, pulse pairs. $\Delta F/F_{sat}$ is the relative pump-induced increase in probe-stimulated Chl fluorescence, which is measured to assess phytoplankton photochemical characteristics. Pump-stimulated Chl fluorescence, phycoerythrin fluorescence and water Raman scattering (displayed as blank triangles, PM, in the lower panel) are also monitored.

date the second laser and to digitize the resulting pump and probe laser-induced fluorescence responses. Laser pulses from the probe (L1) and pump (L2) lasers were directed downward by separate dielectric folding mirrors through the circular port in the belly of the aircraft fuselage to water surface. Both transmitters were Big Sky Laser Technologies model CFR 400 lasers with an output wavelength of 532 nm, an 8.5 ns pulse duration and maximum pulse energy of 160 and 100 mJ for the pump and probe lasers, respectively. The shapes of both the probe and pump beam cross-sections were elliptical. Ground measurements indicated that the dimension of the probe footprint was 4×22 cm at a distance of 150 m. The pump laser head was rotated 40° about its axis and fixed in that position to ensure maximum overlap with the probe beam at a distance of 150 m. A double-lens beam expander, D, (–100 and 200 mm lens focal lengths, respectively) was used to adjust pump beam divergence to provide a footprint that was approximately 50% larger than the probe beam cross-section at the operational distance of 150 m. The increased size of the pump footprint provided tolerance for potential beam misalignment due to mechanical vibration during the flight. A folding mirror, M, was used to center the probe pulse footprint within the larger pump pulse footprint at a distance of 150 m during preflight ground alignment. A 10" Newtonian telescope (f = 4; a custom-built mirror, Muffoletto Optical Company), T, collected the optical response signal from the water column. The signal was spectrally separated with a spectrometer (model MS125, Oriel), SP. Customized rectangular optical fibers located within the focal plane of the spectrometer were used to gather selected spectral bands for laser backscatter (532/7 nm), Chl fluorescence (687/25 nm), water Raman scattering (650/20 nm) and phycoerythrin fluorescence (560/12 and 590/17 nm). (The numbers before and after the slash in the parentheses represent band spectral maximum and width at half max, respectively.) The spectrally separated optical signals were transmitted through the optical fibers to the faces of individual photomultiplier tubes, PMT's, (model H5783-01, Hamamatsu). PMT output pulses were digitized with two 4-channel digital oscilloscopes (model 9450, LeCroy), OS1 and OS2. The waveforms were transmitted to a PC through the GPIB interface and stored on the PC disk drive along with geographic co-ordinates acquired from a Global Positioning System (model 195, Garmin) and sea surface temperature acquired from an infrared radiometer (model KT19, Heimann). A laboratory-built synchronizing PC board provided alternate switching of the pump and probe pulse sequence and delay of the pump-probe pulse pair (see Figure 2) through external triggering of the laser power supplies. The oscilloscopes were triggered by backscatter from the outgoing laser beams. The LIDAR system was installed on a two-engine NOAA Twin Otter aircraft.

Airborne SP-P&P protocol

Laboratory SP-P&P protocol (Chekalyuk et al. 2000) was modified to meet specific requirements for implementation on an airborne LIDAR sensor. The protocol

diagram presented in Figure 2 should be referred to during the following discussion. The P&P protocol requires alternate Chl fluorescence stimulation by a single probe pulse and the combined pump-probe pulse pair (Mauzerall 1972). For practical implementation into the AOL3 LIDAR sensor, it was desirable to operate both lasers at the same 6 Hz pulse repetition rate. Thus, we had to expend a pump pulse that is not required in the original SP-P&P protocol. Accordingly, we devised a strategy to fire the extra pump pulse 5 ms after the initial 'single' probe pulse required in the SP-P&P protocol (see left upper plot in Figure 2). The extra pump pulse provides additional information about chlorophyll (Chl) and phycoerythrin, while maintaining the same high sampling rate as in the original AOL3 configuration.

As illustrated in Figure 2 (upper plot), the water column was alternately excited by probe-pump and pump-probe laser pulse pairs with a repetition rate of 6 Hz, which corresponds to 167 ms delay between pairs. This delay resulted in a 10-m separation between subsequent sampling points along the flight track at the nominal 60 m/s aircraft survey speed. At this velocity, a 5 ms delay in the probe-pump pair (left upper plot in Figure 2) corresponds to a 30 cm airplane translation, which was large enough to avoid spatial overlap of the probe and pump footprints, thus ensuring the integrity of the individual probe and pump measurements. The intensity of probe-induced Chl fluorescence, F, (left dark triangle in the lower plot in Figure 2) is considered to be proportional to the 'original' Chl fluorescence yield if measurements were conducted in the dark (or to the 'actual' Chl fluorescence yield during daytime). The terms 'original' and 'actual' are used in accordance with nomenclature suggested in (van Kooten and Snel 1990).

Previous laboratory investigations showed the 30 μs delay in the pump-probe pair (right upper plot in Figure 2) to be optimal for SP-P&P measurements (Chekalyuk et al. 2000). This delay resulted in only a 0.2 cm footprint displacement between the pump-probe pair at the nominal 60 m/s aircraft speed. This small displacement is negligible compared to the overlap of the beam cross-sections (see above). The intensity of the probe-induced Chl fluorescence signal, F_{sat}, (dark triangle in the lower plot in Figure 2) was higher compared to F because of an increased Chl fluorescence yield due to the pump-induced closure of PS II reaction centers. Spatial variability in Chl concentration and absorption of incident laser energy equally affect the magnitudes of both F and F_{sat} and are eliminated in the relative parameter, $\Delta F/F_{sat} = (F_{sat} - F)/F_{sat}$. Therefore, the $\Delta F/F_{sat}$ magnitude provided a measure of the pump-induced change in Chl fluorescence yield to assess PS II photochemical yield (Genty et al. 1989; Krause and Weis 1991; Govindjee 1995) and its functional absorption cross-section (Mauzerall 1976; Falkowski et al. 1988; Kolber and Falkowski 1993) after applying the EEQ correction (Chekalyuk et al. 2000).

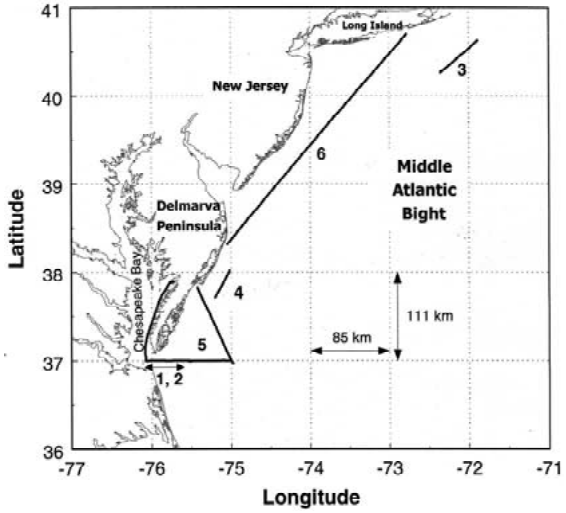

Figure 3. Transect map of SP-P&P airborne LIDAR measurements. Transects are displayed as thick black lines.

In parallel with measuring PS II photochemical characteristics, pump-induced Chl and phycoerythrin fluorescence signals were acquired along with water Raman scattering (marked as 'PM' unfilled triangles in Figure 2). For most of the flight lines flown during the investigation, the pump pulse energy was fixed at its maximum level, thus providing measurements of these parameters consistent with the normal LIDAR-fluorosensor mode (Hoge et al. 1986a, b). The original high-resolution LIDAR data were smoothed to eliminate instrument noise and small-scale structures to facilitate analysis of spatial variability on meso- and synoptic scales. A software package 'Axum 5' (MathSoft) was used for the data analysis and graphic representations.

Results and discussion

Six airborne missions were conducted with a prototype of the P&P LIDAR between the 8th of March and the 18th of March 1999 in the Middle Atlantic

Bight and Chesapeake Bay area with a total transect length of 2280 km. A transect map is presented in Figure 3. Several separate, but related investigations were pursued within this flight series. The results of these investigations are discussed separately within this section of the paper.

Airborne LIDAR study of natural variability in excessive energy quenching

A laboratory study conducted with phytoplankton cultures and seawater revealed that excessive energy quenching, EEQ, must be well pronounced in the SP-P&P LIDAR measurements acquired with 10 ns laser pulse stimulation (Chekalyuk et al. 2000). Thus, the airborne SP-P&P data need to be corrected in order to accurately estimate PS II photochemical parameters. This correction procedure requires knowledge of the EEQ rate constant, which was found to be species-dependent (Chekalyuk et al. 2000) and, therefore, might vary because of changes in phytoplankton composition over large aquatic areas. One of the main technological issues of the airborne SP-P&P LIDAR test was to evaluate the EEQ effect and its spatial/temporal variability in order to specify and optimize the measurement protocol for an operational airborne SP-P&P LIDAR system. Note that the airborne LIDAR measurement might result in EEQ variation because of the lens effect of the water surface and variability in water attenuation. Therefore, it was necessary to conduct a 'real-world' test of laboratory EEQ findings presented in (Chekalyuk et al. 2000).

The prototype P&P LIDAR implementation on the NASA AOL3 LIDAR did not provide the capability to change laser pulse energy on successive pulses. In order to investigate the change in Chl fluorescence yield at different probe pulse energy settings, it was necessary to locate a phytoplankton patch and then to fly a series of 5–6 repeated passes over the feature along the same flight track while changing probe pulse energy setting between each pass. This experiment scenario was repeated along four transect lines of 20–50 km in length located near the mouth of the Chesapeake Bay and at two other locations within the Middle Atlantic Bight between the 11th of March and the 18th of March 1999 (Transects 1–4 in Figure 3). Each flight series was started at least 1 h after sunset to provide dark adaptation of the phytoplankton photosynthetic apparatus. Prior to the flight series, ground measurements were conducted at a distance of 150-m to ensure an appropriate pass-to-pass range of

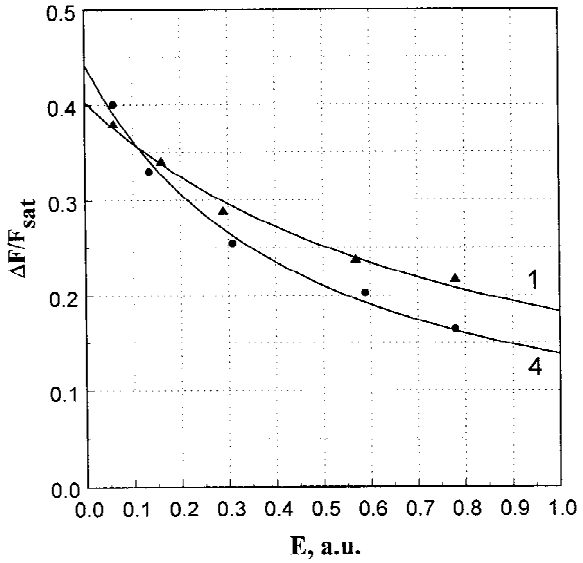

Figure 4. Examples of airborne LIDAR measurements of EEQ decline in relative variable fluorescence, $\Delta F/F_{sat}$, plotted as a function of increasing probe fluence, E. The latter is presented in arbitrary units, a.u. Symbols represent transect-mean $\Delta F/F_{sat}$ magnitudes versus E settings along Transects 1 and 4 in Figure 3, respectively. The pump fluence was fixed at the PS II saturating level. The solid lines display results of a non-linear regression of the experimental data with equation $\Delta F/F_{sat} = \Phi_{Po}(1 + (1 - \Phi_{Po})R_Q E)^{-1}$.

fluence settings. The pump pulse energy was fixed at its maximum level, which provided complete PS II saturation in the sub-surface water column and, accordingly, maximal $\Delta F/F_{sat}$ magnitudes. This aspect was verified by special measurements to be discussed in the next section.

Synoptic-scale EEQ variability was a primary matter of interest in this experiment, therefore the transect data sets of 30–50 km length were separated by a few-hundred kilometer distance and the $\Delta F/F_{sat}$ data were averaged for each transect pass. Examples of experimental curves developed from Transects 1 and 4 (Figure 3) are displayed in Figure 4. Discrete points represent transect-mean $\Delta F/F_{sat}$ magnitudes versus respective probe pulse fluence settings, E. The latter is presented in relative units. Based on the ground LIDAR calibration, E = '1' corresponds to a fluence magnitude of 16.7 μmol quanta m^{-2} (or 0.4 mJ/cm^2 at 532 nm wavelength) at the water surface. Energy losses related to beam propagation through the atmosphere and water column are not considered in this estimate. The solid lines are best fits of the experimental points using equation $\Delta F/F_{sat} = \Phi_{Po}(1 + (1 - \Phi_{Po})R_Q E)^{-1}$, which can be derived by rearrangement of Equation (16) in (Chekalyuk et al. 2000). As it is

Table 1. Transect-mean results of airborne SP-P&P LIDAR measurements. Data on the EEQ effect are presented on the gray-shaded background. 'R_Q / SE' and 'Φ_{Po} / SE' rows tabulate magnitudes of the EEQ relative rate parameter, R_Q, and PS II maximum potential photochemical yield, Φ_{Po}, along with their standard error of estimates, SE. The lower, non-shaded part of the table, presents results of independent measurements of Φ_{Po} and the PS II functional absorption cross-section, σ_{PSII}, over corresponding transects. For each data set, the 'R^2 / SD' rows display magnitudes of the correlation coefficient, R^2, and the corresponding standard deviation of errors, SD

Transect	1	2	3	4
Transect location (Figure 3)	Chesapeake Bay mouth	Chesapeake Bay mouth	South-east of Long Island	East of Delmarva Peninsula
Date	11th March 1999	16th March 1999	17th March 1999	18th March 1999
R_Q / SE, a.u.	2.01 / 0.20	1.98 / 0.192.59 / 0.10	2.59 / 0.10	3.96 / 0.51
Φ_{Po} / SE	0.40 / 0.01	0.38 / 0.01	0.43 / 0.01	0.44 / 0.02
R^2 / SD	0.99 / 0.01	0.99 / 0.01	1.00 / 0.00	0.99 / 0.01
σ_{PSII} / SE, a.u.	–	8.3 / 1.7	–	5.7 / 0.02
Φ_{Po} / SE	–	0.36 / 0.02	–	0.42 / 0.01
R^2 / SD	–	0.97 / 0.02	–	0.99 / 0.02

evident from the equation, the intercepts of these lines with the vertical axis at E = 0 in Figure 4 provide values of Φ_{Po}. The magnitudes of the Φ_{Po} and R_Q parameters estimated by the non-linear regression are tabulated in the gray-shaded section of Table 1. Since the measurements were conducted under dark-adapted conditions with the PS II-saturating pump pulse, the magnitude of Φ_{Po} parameter provides an estimate of the maximum potential PS II photochemical yield for phytoplankton in the sub-surface water column. Absolute remote measurements of pump and probe fluences in the near-surface water column were not feasible during these initial field tests of the SP-P&P protocol. As a result, the R_Q data as well as magnitude of the σ_{PSII} values in Table 1 (see below) are presented in arbitrary units corresponding to a '0–1' range in fluence variation.

Data presented in Figure 4 and Table 1 indicate that the simplified EEQ model (Chekalyuk et al. 2000) adequately encompasses results of the airborne SP-P&P LIDAR measurements and can therefore be used for the EEQ data correction. The quenching effect was well pronounced over the range of probe fluence variation (note an almost 3-fold maximal $\Delta F/F_{sat}$ decline in Figure 4), and there was a noticeable difference in the EEQ magnitude between the three surveyed areas. A 2-fold difference in R_Q magnitudes (and, therefore, in EEQ rates) was found over a 100-km distance (Transects 1, 2 and 4), while the PS II photochemical yield, Φ_{Po}, did not show significant variations (Table 1). Since the measurements were not conducted simultaneously, both spatial and temporal R_Q changes might potentially cause this difference. Note that the time interval between measurements along Transects 2 and 4 was 2 days. On the other hand, remarkably identical (within experimental error) R_Q values were measured in the Chesapeake Bay mouth with a longer, 5-day delay (compare columns 1 and 2 in Table 1). We believe, therefore, the 2-fold difference in R_Q should be attributed rather to spatial than to temporal factors. Overall, the R_Q variability observed in the three surveyed areas is consistent with results of laboratory studies of phytoplankton cultures and seawater samples reported in (Chekalyuk et al. 2000). It is apparent that an operational SP-P&P protocol should provide continuous R_Q monitoring to produce an accurate EEQ data correction.

An increase in probe pulse energy results in more intensive F and F_{sat} fluorescence signals, but causes a corresponding decline in the $\Delta F/F_{sat}$ parameter, as is evident from Figure 4. In the prototype LIDAR configuration described above, an acceptable signal-to-noise ratio in the $\Delta F/F_{sat}$ data was observed at probe laser pulse energy levels corresponding to a fluence range of '0.1'–'0.3' on the arbitrary scale used in Figure 4. Based on the data presented in Figure 4 and Table 1, the EEQ correction resulted in 10–30% increases in the magnitude of $\Delta F/F_{sat}$ measured in this fluence range. This correction procedure was applied to all SP-P&P data acquired at night and it appeared to provide reasonable estimates of the PS II photochemical yield. With regard to temporal R_Q variability, the above-mentioned reproduction of R_Q magnitude over the 5-day period of sampling in the Chesapeake Bay mouth suggests that no major changes occurred in the phytoplankton composition over this period (see the multiparameter LIDAR data in Figure 7 for more details).

Airborne measurements of PS II absorption cross-section and photochemical yield

The second group of experiments was aimed at exploring the feasibility of simultaneous airborne measurements of the PS II functional absorption cross-section, σ_{PSII}, and determining its maximal potential photochemical yield, Φ_{Po}. An additional objective of this investigation was to verify that the maximum pump energy setting utilized during the EEQ rate measurements (discussed in the preceding section) provided complete saturation of PS II photochemistry in the near-surface water column. This was accomplished by measuring the induction in variable fluorescence with increasing pump pulse fluence, while maintaining the fixed probe pulse fluence and delay as described elsewhere (Mauzerall 1976; Falkowski et al. 1988; Chekalyuk et al. 2000). Since the prototype P&P implementation on the NASA AOL3 LIDAR did not provide the capability to change laser pulse energy on successive pulses, it was necessary to gather the data on 5–6 repeated passes along the same flight track, while changing pump pulse energy setting between each pass. We estimate that the maximum pump pulse fluence on the ocean surface was 0.25 mJ/cm^2 based on the measured maximum pulse energy of the pump laser and the cross-sectional area of pump beam (see the 'SP-P&P LIDAR prototype' section above). This corresponds to the required PS II saturating fluence

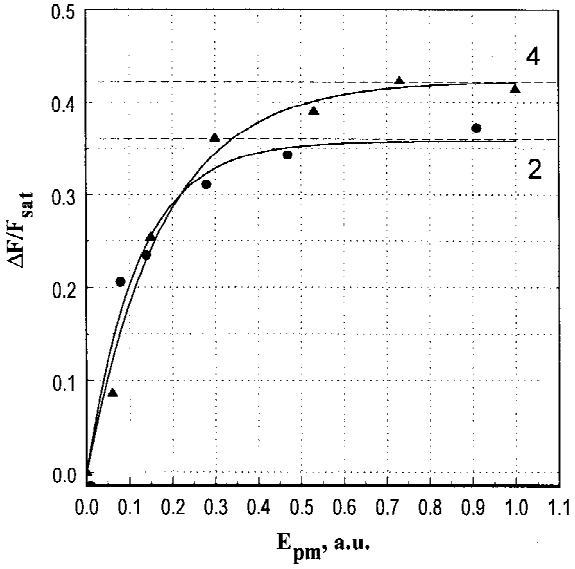

Figure 5. Examples of airborne LIDAR data analyzed for assessment of PS II photochemical quantum yield, Φ_{Po}, and its functional absorption cross-section, σ_{PSII}. The symbols represent transect-mean EEQ-corrected $\Delta F/F_{sat}$ magnitudes plotted as a function of pump pulse fluence, E_{pm} along Transects 2 and 4 in Figure 3, respectively. The solid lines display results of a non-linear regression with the function $\Phi_{Po}(1 - \exp(-\sigma_{PSII}E_{pm}))$. The dashed lines indicate the corresponding retrieved Φ_{Po} magnitudes.

magnitude of 0.2 mJ/cm^2 specified for phytoplankton in (Chekalyuk et al. 2000). During this investigation, the probe laser energy was fixed at a level corresponding to a fluence magnitude of about '0.1' on the relative scale described in the previous section.

These measurements were conducted along Transects 2 and 4 (Figure 3) immediately after the series of EEQ rate measurements. Results from the data processing are displayed in Figure 5. The discrete points represent the mean magnitudes of the $\Delta F/F_{sat}$ parameter from each transect versus the pump pulse fluence, $E_{pm,}$ (relative units). The solid lines are a best fit of the experimental points using function $\Phi_{Po}(1 - \exp(-\sigma_{PSII}E_{pm}))$ in accordance with Equation (11) in Chekalyuk et al. (2000). Prior to the analysis, the $\Delta F/F_{sat}$ data were corrected for the EEQ effect produced by sub-saturating probe pulses. This correction is based on Equation (15) in Chekalyuk et al. (2000) and the R_Q magnitudes measured over the corresponding transects (see Table 1). The magnitudes of Φ_{Po} and σ_{PSII} derived from the non-linear regression are tabulated in the lower non-shaded portion of Table 1. The σ_{PSII} values are presented in arbitrary units for the same reason given for the R_Q data above.

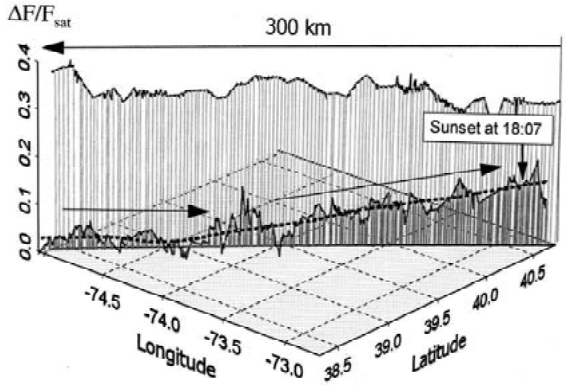

Figure 6. Results of before- and after-dusk airborne LIDAR monitoring of the $\Delta F/F_{sat}$ parameter between Delmarva Peninsula and Long Island (Transect 6 in Figure 3). The lower trace represents $\Delta F/F_{sat}$ measurements conducted between 17:08 and 18:19. Sunset took place at 18:07. The dashed line denotes smoothed $\Delta F/F_{sat}$ data for trend evaluation. The upper trace displays the $\Delta F/F_{sat}$ magnitudes measured between 23:56 and 01:33. The $\Delta F/F_{sat}$ data are not EEQ-corrected.

As evident from Figure 5 and the high correlation values presented in Table. 2, the above function, $\Phi_{Po}(1 - \exp(-\sigma_{PSII}E_{pm}))$, well describes the results of the airborne LIDAR measurements, and indicates that the SP-P&P protocol can, therefore, be used to remotely assess the Φ_{Po} and σ_{PSII} parameters. Saturation trends in the $\Delta F/F_{sat}$ rise are evident in both data sets presented in Figure 5. In each case, the experimentally measured $\Delta F/F_{sat}$ values acquired at the maximum pump pulse energy level reached the Φ_{Po} estimates obtained by the best-fit regression procedure (see Table 1). Therefore, this maximum pump pulse energy setting provided sufficient pump fluence to completely saturate the PS II photochemical charge separation within the upper water column. In particular, this finding confirms correctness of the pump laser energy setting in the EEQ series described in the previous section. This maximal pump setting was specified during the prolonged airborne SP-P&P measurements conducted in the area during prototype LIDAR tests (for example, see Figure 6).

An estimate, based on maximum pulse laser energy levels and the beam cross-sectional areas presented in the 'SP-P&P LIDAR prototype' section, indicates that the maximum pump and probe pulse fluences were of the same order of magnitude from the 150 m flight altitude. Thus, the probe fluence variation range in the experiments described in the preceding section (e.g. see Figure 4) can indeed be qualified as PS II sub-saturating. Note that the Φ_{Po} estimates obtained during two independent experiments along Transects 2 and 4 are very close (0.38 vs. 0.36, and 0.43 vs. 0.42, respectively; see shaded and non-shaded areas in Table 1). Considering spatial variability, the differences in σ_{PSII} magnitudes appeared to be more pronounced than the differences in Φ_{Po} magnitudes (32% vs.14%). Apparently, any generalization regarding their variability must await a representative database to be acquired.

Before- and after-dusk LIDAR measurements of variable fluorescence

A pronounced daytime decrease in variable fluorescence and its recovery after sunset were observed during experiments conducted with the SP-P&P LIDAR. An example of such observations during a 300 km LIDAR survey between Delmarva Peninsula and Long Island (Transect 6 in Figure 3) is presented in Figure 6. The northeast bound measurements were acquired between 17:08 and 18:19 EST, while the southwest bound flight over the same track was flown between 23:56 and 01:33 EST (17–18th March 1999). Sunset took place near the end part of the first transect at 18:07. Very low $\Delta F/F_{sat}$ magnitudes were found in the initial portion of northeast bound, 'before-sunset', transect. However, a gradual increase in the average $\Delta F/F_{sat}$ values, from 0.02 to 0.16, can be seen in the northeast direction beginning near 39° N. The night southwest bound transect, conducted a few hours after sunset, indicated a quite homogeneous $\Delta F/F_{sat}$ distribution over most of the flight line with magnitudes varying in a range of 0.3–0.4. The homogeneous $\Delta F/F_{sat}$ distribution found in the night pass suggests that the gradual $\Delta F/F_{sat}$ rise observed in the northeast transect as sunset approached was more likely caused by a gradual increase in the PS II photochemical efficiency with decreasing ambient light than by its actual spatial variability. Similar phenomena were observed during a 298 km transect measurement around the lower portion of the Delmarva Peninsula including a portion of the Chesapeake Bay south of 38 ° N (Transect 5 in Figure 3). The $\Delta F/F_{sat}$ parameter showed near-zero magnitudes during afternoon measurement and meso-scale variations in a range of 0.3–0.5, 1 h after the sunset.

The observed phenomena are consistent with data on vertical profiling of variable fluorescence within the photic layer (Kolber and Falkowski 1993; Falkowski and Kolber 1995) and with observations of diurnal variations in phytoplankton PS II photochemical yield

in the subsurface water column conducted with a shipboard P&P LIDAR system (Chekalyuk and Gorbunov 1994a, b). Typically, about 80% of the airborne LIDAR response signal comes from the upper 3–5 m of the water column where the daytime decline in PS II photochemical activity is most pronounced (for example, see Figure 10 in Falkowski and Kolber (1995)). Part of this decline is caused by various non-photochemical quenching mechanisms, such as energy-dependent and 'photoinhibitory' quenching (Krause and Weis 1991). A decrease in photochemical quenching due to the 'dynamic' closure of a fraction of the PS II reaction centers under ambient light also appears to affect both photochemical and fluorescence yields (e.g. see data in Kolber and Falkowski (1993)). A combination of these mechanisms may result in a more than 10-fold decline in the actual daytime PS II photochemical yield within the subsurface seawater layer compared to its maximum potential magnitude in a dark-adapted state (Chekalyuk and Gorbunov 1994b; Falkowski and Kolber 1995). It takes up to ~1–2 h to complete after-sunset PS II recovery in the near-surface water column (Chekalyuk and Gorbunov 1994b). This explains the gradual PS II recovery processes observed with the approach of sunset in the northeast portion of the transect in Figure 6 and corresponds to the delay between sunset and beginning of the night measurement in the second example.

This data demonstrates that a significant improvement in LIDAR measurement accuracy would be required in order to provide reliable daytime monitoring of PS II photochemical activity because of the small relative difference between the actual and maximal Chl fluorescence yield under bright ambient light. Also, the interpretation of daytime P&P LIDAR data would be complicated because of a variety of mechanisms involved in regulating the PS II functionality under ambient light. Potential 'overlap' of diurnal temporal and synoptic-scale spatial variability, as evident from the above example, might cause additional problems in data interpretation. Therefore, the most reasonable approach at the current research stage appears to be to acquire measurements of the potential magnitudes of the PS II photochemical yield and functional absorption cross-section under dark conditions. This sampling strategy would permit the acquisition of a unique, and inaccessible by other techniques, database covering the variability of PS II photochemical characteristics in the ocean over a wide range of spatial and temporal scales. Coupled with progress in our understanding of the regulation of PS II photochemical activity under ambient light, such a database could lead to the development of an adequate model for remote assessment of daytime photosynthetic processes within the ocean photic layer, including primary productivity.

SP-P&P multiparameter LIDAR measurements

The ocean is a highly-dynamic media with complex interactions between various physical and biogeochemical processes (Kirk 1994; Falkowski and Raven 1997). An advantage of the SP-P&P LIDAR protocol is that it permits the simultaneous acquisition of a quite informative data set for a more complete characterization of the surveyed area. As discussed above (see 'Airborne SP-P&P protocol' section and Figure 2), pump-stimulated Chl and phycoerythrin fluorescence signals and water Raman scattering can be monitored along with the variable fluorescence parameter, $\Delta F/F_{sat}$. Chl and phycoerythrin (an accessory pigment found in certain phytoplankton and marine bacteria) fluorescence, normalized by the Raman scattering, allows estimation of pigment concentration (Hoge and Swift 1981). Comparative analysis of phycoerythrin fluorescence measured at 590 and 560 nm permits distinguishing between different strains of cyanobacteria (Hoge et al. 1998). Taken together with Chl fluorescence data, this capability ensures some potential for remote phytoplankton taxonomic analysis. The $\Delta F/F_{sat}$ parameter provides information about the maximum potential (or actual, if measured under ambient light) PS II photochemical efficiency and its functional absorption cross-section. Coupled with the Chl concentration data, the PS II photochemical parameters provide a basis for estimation of photosynthetic rate parameters by using a biophysical model (Kolber and Falkowski 1993; Falkowski and Kolber 1995).

Though the reported research was mainly focused on the airborne implementation of the pump-and-probe technology *per se*, we tested the feasibility of concurrent acquisition of a multiparameter data set. An example of such measurements gathered near the Chesapeake Bay mouth (transect location is marked as '1, 2' in Figure 3) is displayed in Figure 7. It represents part of the data acquired during a flight around the southern part of Delmarva Peninsula on the night of the 16th of March 1999. The data set was obtained during a series of 14-min flights over the 40-km transect. The distribution of the maximum potential PS II photochemical yield, Φ_{Po}, was calculated from the measured $\Delta F/F_{sat}$ data after applying an EEQ correc-

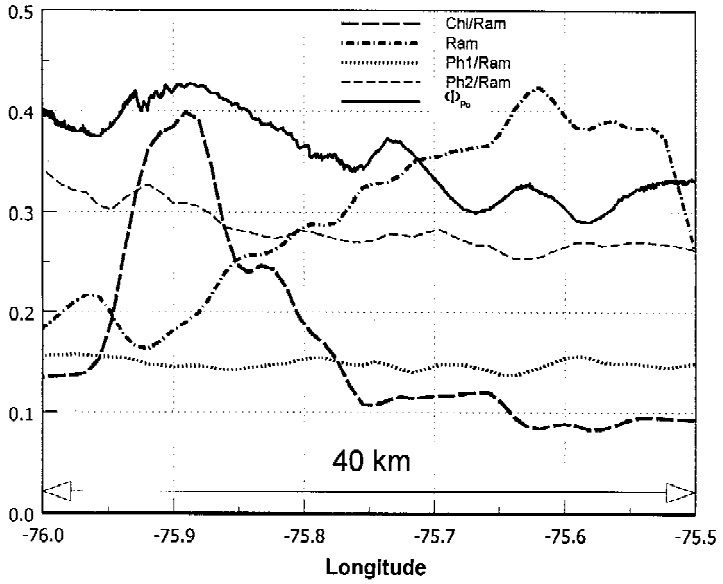

Figure 7. An example of a multiparameter SP-P&P LIDAR survey conducted on 16th March 1999 in the vicinity of the Chesapeake Bay mouth along Transects 2 (see Figure 3). 'Ram', 'Chl/Ram', 'Ph1/Ram' and 'Ph2/Ram' denote pump-stimulated water Raman scattering, Chl fluorescence, and phycoerythrin fluorescence at 560 and 590 nm, respectively (all in relative units). The Chl and phycoerythrin fluorescence signals have been normalized by water Raman scattering. Φ_{Po} is the estimated PS II maximum potential photochemical yield based on EEQ-corrected $\Delta F/F_{sat}$ LIDAR measurements.

tion using R_Q magnitudes measured along the same transects (see Table 1). Chl and phycoerythrin fluorescence signals presented in Figure 7 were normalized by the concurrently measured Raman scattering.

A phytoplankton patch with a 4-fold increase in Chl fluorescence was found in the western portion of the transect during the survey (thick dashed line). A profile of PS II photochemical yield (solid line), Φ_{Po}, indicates a moderate potential PS II photochemical efficiency with low spatial variability and a gradual increase (0.3–0.4) toward the west in the direction of the Chesapeake Bay mouth, where the phytoplankton patch was located. Thus, only 30–40% of the absorbed light energy could be potentially used to drive photochemical charge separation in the PS II reaction centers, while the maximum photochemical efficiency for phytoplankton was found to be 65% (Falkowski and Kolber 1995). Based on this data and Equation (5) in Chekalyuk et al. (2000), a proportion of photochemically active PS II reaction centers can be estimated as 26%–36%. A similar increase toward the western end of the flight line was observed in phycoerythrin fluorescence measured at 590 nm (thin dashed line in Figure 7), while phycoerythrin fluorescence measured at 560 nm (dotted line) indicated no significant changes along the transect. This trend indicates relative increase in abundance of phycoerythrobilin- vs. phycourobilin-containing cyanobacteria, typical for coastal waters (Hoge et al. 1998). Both the Chl and phycoerythrin fluorescence increases were well correlated spatially with a 50% drop in Raman scattering signal (dashed-dotted line in Figure 7). The observed decrease in Raman scattering is attributed to increased absorption due to the elevated concentrations of phytoplankton pigments and dissolved organic matter near the Chesapeake Bay mouth.

Conclusion

Results of the first airborne SP-P&P LIDAR tests, reported in this communication, have demonstrated the feasibility and potential of technology for studying spatial and temporal variability in phytoplankton photochemical characteristics. Unfortunately, we could not compare photochemical parameters independently measured with the LIDAR and commercial shipboard fast-repetition-rate fluorometer because of software-related failure of the latter, but we plan to conduct extensive comparative analysis during our future activities. Meanwhile, the consistency of data obtained in these LIDAR experiments along with results of preliminary theoretical and experimental studies, as well

as a reasonable range of estimated Φ_{Po} magnitudes, has further stimulated our research efforts to transfer P&P techniques from a research environment into operational implementation.

With respect to technological plans, our current major focus is on the development of an advanced LIDAR system capable of combined single-transect operational measurements of photochemical and 'conventional' LIDAR parameters. We have already found and recently verified a technological solution, which allows reliable control over the pump pulse energy on a pulse-to-pulse basis, thus making the development of an operational SP-P&P LIDAR feasible. Although the SP-P&P approach provides higher signal compared to a conventional P&P protocol, a solution for sensitivity improvement still needs to be found in order to conduct operational high-resolution LIDAR measurements of phytoplankton photochemical characteristics.

In the research area, a representative database covering the variability of phytoplankton photochemical parameters over different spatial/temporal scales must be acquired. Technologically, this would allow further optimization of the LIDAR measuring protocol. Based on preliminary data, PS II photochemical yield seems to have less pronounced meso-scale spatial variability compared to pigment fluorescence. If this would be generally confirmed based on LIDAR measurements in different areas and seasons, it should allow reducing the sampling frequency or sensitivity requirements when measuring photochemical characteristics.

Generally speaking, studying the spatial/temporal variability is of great importance for marine research and environmental monitoring. At this point, the SP-P&P LIDAR technique provides unique possibilities of remote multiparameter biomonitoring of complex phenomena over a wide range of temporal/spatial scales. Due to the use of an airborne platform, the measurement protocol can be flexibly adjusted to provide adequate coverage while investigating processes. In particular, the novel airborne SP-P&P LIDAR technology has the potential to bridge the gap between satellite and shipboard techniques for estimating phytoplankton photosynthetic activity. This would be the major application of an operational airborne P&P LIDAR system. The advantage of such an approach over existing techniques is that it would be based on direct high-resolution *measurements* of photosynthetic characteristics instead of indirect *estimates*.

An important step in this direction would be finding a technological solution to provide measurements of the PS II functional absorption cross-section, σ_{PSII}, in absolute units. In fact, P&P LIDAR is the only remote sensing instrument potentially capable of direct measurement of phytoplankton photosynthetic-specific absorption. Such information, if available, could be used along with data on PS II photochemical quantum yield and Chl concentration for estimating variability in the rate of PS II photochemical electron transport (Kolber and Falkowski 1993) over large aquatic areas. Further development of this approach might result in the development of a new remote sensing technology for assessment of photosynthetic rate parameters, including phytoplankton primary productivity.

Acknowledgements

The authors would like to thank Prof. Paul Falkowski and Dr Zbigniew Kolber for useful discussions. The authors also thank Carl Schirtzinger and Alan Waller for their assistance in AOL3 modification and ground tests, as well as NOAA pilots Michele Finn and Phil Hall for excellent piloting of the aircraft. We are grateful for the support of Dr Janet Campbell and Dr John Marra, former and current Ocean Biology Program Scientists at NASA Headquarters, and to Drs Mary Culver and Dave Eslinger of the NOAA Coastal Services Center for their support in the conduct of the field experiments. Dr Alexander Chekalyuk was supported by an award from National Research Council (USA).

References

Chekalyuk AM and Gorbunov MYu (1994a) Pump-and-probe LIDAR fluorosensor and its applications for estimates of phytoplankton photosynthetic activity. In: Second Thematic Conference on Remote Sensing for Marine and Coastal Environments, pp 389–400. New Orleans, USA, 31 January – 2 February 1994 ERIM Publ., Ann Arbor, Michigan

Chekalyuk AM and Gorbunov MYu (1994b) Diel variability of *in vivo* chlorophyll fluorescence in near-surface water layer. SPIE 2258: 140–151

Chekalyuk AM, Olson RJ and Sosik HM (1996) Pump-during-probe fluorometry of phytoplankton: Group-specific photosynthetic characteristics from individual cell analysis. SPIE 2963: 840–845

Chekalyuk AM, Hoge FE, Wright CW and Swift RN (2000) Short-pulse pump-and-probe technique for airborne laser assessment of Photosystem II photochemical characteristics. Photosynth Res 66: 33–44 (this issue)

Falkowski PG and Kolber Z (1995) Variations in chlorophyll fluorescence yields in phytoplankton in the world oceans. Aust J Plant Physiol 22: 341–355

Falkowski PG and Raven JA (1997) Aquatic Photosynthesis. Blackwell Science, Malden

Falkowski PG, Fujita Y, Ley A and Mauzerall D (1986) Evidence for cyclic electron flow around Photosystem II in *Chlorella pyrenoidosa*. Plant Physiol 81: 310–312

Falkowski PG, Kolber Z and Fujita Y (1988) Effect of redox state on the dynamics Photosystem II during steady-state photosynthesis in eucaryotic algae. Biochim Biophys Acta 933: 432–443

Falkowski PG, Ziemann D, Kolber Z and Bienfang PK (1991) Role of eddy pumping in enhancing primary production in the ocean. Nature 352: 55–58

Field C, Behrenfeld MJ, Randerson JT and Falkowski PG (1998) Primary production of the biosphere: Integrating terrestrial and oceanic components. Science 281: 237–240

Geider R, Greene R, Kolber Z, MacIntyre HL and Falkowski PG (1993) Fluorescence assessment of the maximum quantum efficiency of photosynthesis in the western North Atlantic. Deep-Sea Res 40: 1205–1224

Genty B, Briantis J-M and Baker N (1989) The relationship between the quantum yield of photosynthetic electron transport and quenching of chlorophyll fluorescence. Biochim Biophys Acta 990: 87–92

Govindjee (1995) Sixty-three years since Kautsky: Chlorophyll *a* fluorescence. Aust J Plant Physiol 22: 131–160

Hoge FE and Swift RN (1981) Airborne simultaneous spectroscopic detection of laser-induced water Raman backscatter and fluorescence from chlorophyll *a* and other naturally occurring pigments. Appl Opt 20: 3197–3205

Hoge FE, Berry RE and Swift RN (1986a) Active-passive airborne ocean color measurements. 1: Instrumentation. Appl Opt 25: 39–47

Hoge FE, Swift RN and Yungel JK (1986b) Active-passive airborne ocean color measurement. 2: Applications. Appl Opt 25: 48–57

Hoge FE, Wright CW, Kana TM, Swift RN and Yungel JK (1998) Spatial variability of oceanic phycoerythrin spectral types derived from airborne laser-induced fluorescence emissions. Appl Opt 21: 4744–4749

Johnson B, Higgs C, Primmerman C, Mandra R, Jeys T, DeFeo W, Grey P and Rowe G (1995) Airborne LIDAR measurements of phytoplankton abundance and productivity in New England coastal waters. In: Third Thematic Conference on Remote Sensing for Marine and Coastal Environments, pp 819–832

Kirk JTO (1994) Light and Photosynthesis in Aquatic Ecosystems. Cambridge University Press, Cambridge

Kolber Z and Falkowski PG (1993) Use of active fluorescence to estimate phytoplankton photosynthesis in situ. Limnol Oceanogr 38: 1646–1665

Kolber Z, Wyman KD and Falkowski PG (1990) Natural variability in photosynthetic energy conversion efficiency: A field study in the Gulf of Maine. Limnol Oceanogr 35: 72–79

Kolber Z, Barber RT, Coale KH, Fitzwater SE, Greene RM, Johnson KS, Linley S and Falkowski PG (1994) Iron limitation of phytoplankton photosynthesis in the equatorial Pacific Ocean. Nature 371: 145–149

Kolber Z, Prazil O and Falkowski PG (1998) Measurements of variable chlorophyll fluorescence using fast repetition rate techniques: Defining methodology and experimental protocols. Biochim Biophys Acta 1367: 88–106

Kramer DM, Robinson HR and Crofts AR (1990) A portable multiflash kinetic fluorimeter for measurement of donor and acceptor reactions of Photosystem II in leaves of intact plants under field conditions. Photosynth Res 26: 181–193

Krause GH and Weis E (1991) Chlorophyll fluorescence and photosynthesis: The basics. Ann Rev Plant Physiol 42: 313–349

Mauzerall D (1972) Light-induced fluorescence changes in *Chlorella*, and the primary photoreactions for production of oxygen. Proc Nat Acad Sci 69: 1358–1362

Mauzerall D (1976) Multiple excitations in photosynthetic systems. Biophys J 16: 87–91

Olson RJ, Chekalyuk AM and Sosik HM (1996) Phytoplankton photosynthetic characteristics from fluorescence induction assays of individual cells. Limnol Oceanogr 41: 1253–1263

Olson RJ, Sosik HM and Chekalyuk AM (1999) Photosynthetic characteristics of marine phytoplankton from pump-during-probe fluorometry of individual cells at sea. Cytometry 37: 1–13

Schreiber U, Groberman L and Vidaver W (1975) Portable, solid-state fluorometer for measurement of chlorophyll fluorescence induction in plants. Rev Sci Instrum 46: 538–542

Schreiber U, Neubauer C and Schliwa U (1993) PAM fluorometer based on medium-frequency pulsed Xe-flash measuring light: A highly sensitive new tool in basic and applied photosynthesis research. Photosynth Res 36: 65–72

van Kooten O and Snel JFH (1990) The use of chlorophyll fluorescence nomenclature in plant stress physiology. Photosynth Res 25: 147–150